Journal of Cerebral Blood Flow & Metabolism (2012) 32, 745–758

www.jcbfm.com

Evolution of the dynamic changes in functional cerebral oxidative metabolism from tissue mitochondria to blood oxygen

Alberto L Vazquez[1], Mitsuhiro Fukuda[1] and Seong-Gi Kim[1,2]

[1]*Neuroimaging Laboratory, Department of Radiology, University of Pittsburgh, Pittsburgh, Pennsylvania, USA;* [2]*Department of Neurobiology, University of Pittsburgh, Pittsburgh, Pennsylvania, USA*

The dynamic properties of the cerebral metabolic rate of oxygen consumption (CMR_{O2}) during changes in brain activity remain unclear. Therefore, the spatial and temporal evolution of functional increases in CMR_{O2} was investigated in the rat somato-sensory cortex during forelimb stimulation under a suppressed blood flow response condition. Temporally, stimulation elicited a fast increase in tissue mitochondria CMR_{O2} described by a time constant of ~1 second measured using flavoprotein autofluorescence imaging. CMR_{O2}-driven changes in the tissue oxygen tension measured using an oxygen electrode and blood oxygenation measured using optical imaging of intrinsic signal followed; however, these changes were slow with time constants of ~5 and ~10 seconds, respectively. This slow change in CMR_{O2}-driven blood oxygenation partly explains the commonly observed post-stimulus blood oxygen level-dependent (BOLD) undershoot. Spatially, the changes in mitochondria CMR_{O2} were similar to the changes in blood oxygenation. Finally, the increases in CMR_{O2} were well correlated with the evoked multi-unit spiking activity. These findings show that dynamic CMR_{O2} calculations made using only blood oxygenation data (e.g., BOLD functional magnetic resonance imaging (fMRI)) do not directly reflect the temporal changes in the tissue's mitochondria metabolic rate; however, the findings presented can bridge the gap between the changes in cellular oxidative rate and blood oxygenation.
Journal of Cerebral Blood Flow & Metabolism (2012) **32,** 745–758; doi:10.1038/jcbfm.2011.198; published online 1 February 2012

Keywords: CMR_{O2}; cortex; flavoprotein; fMRI; hemoglobin; metabolism; optical; oxygen; P_{O2}

Introduction

The brain is highly reliant on adequate blood supply to sustain its function. Oxygen and glucose are the primary metabolic substrates and these are delivered to brain tissue mostly at cerebral capillaries. Most of the oxygen transported by blood is bound to hemoglobin and as the oxygen tension of the surrounding environment decreases, oxygen dissociates and crosses into tissue. Oxygen is then consumed in cellular mitochondria as part of oxidative metabolism, which supplies sufficient energy to sustain essential cellular functions. Further, changes in brain activity dynamically modulate the tissue's metabolic rate. The seminal work by Fox *et al* (1988) was the first to report that increases in brain activity produced significant increases in the cerebral metabolic rate of glucose consumption and disproportionately smaller increases in the cerebral metabolic rate of oxygen consumption (CMR_{O2}). These findings introduced the notion that the brain's energetic needs to satisfy increases in activity may be partly supplied by nonoxidative means (i.e., glycolysis). A large number of studies have been performed since which report larger steady-state increases in CMR_{O2} with increases in brain activity (for a review, see Shulman *et al*, 2001); however, the dynamic properties of oxidative metabolism during changes in brain activity remain unclear.

Most *in vivo* assessments of activation-evoked changes in CMR_{O2} rely on tissue or blood oxygenation measurements and, therefore, are indirect. Since evoked increases in neural activity cause increases in both CMR_{O2} and cerebral blood flow (CBF), which are well known to oppositely influence the changes in tissue and blood oxygenation, it is essential to isolate the changes in oxygenation produced by CMR_{O2} from those produced by CBF. Hence, methods that

Correspondence: Dr AL Vazquez, McGowan Institute Room 159, 3025 East Carson Street, Pittsburgh, PA 15203, USA.
E-mail: alv15@pitt.edu
This work was supported by NIH grants F32-NS056682, K01-NS066131, R01-NS044589, R21-EB006571, and R01-EB003375.
Received 19 July 2011; revised 9 December 2011; accepted 15 December 2011; published online 1 February 2012

calculate CMR_{O2} from blood oxygenation data require additional information to account for the changes in oxygenation produced by changes in CBF alone (Davis *et al*, 1998; Kim *et al*, 1999). Studies using this method have suggested that neural activity-induced increases in CMR_{O2} are temporally similar to the concomitant increases in CBF (Davis *et al*, 1998; Ances *et al*, 2001; Obata *et al*, 2004; Herman *et al*, 2009). This observation is largely due to the significant contribution of CBF on the changes in blood oxygenation, which overwhelm the changes in oxygenation due to CMR_{O2} (Buxton *et al*, 2004; Chiarelli *et al*, 2007). In addition, this method typically assumes that the oxygen extracted from blood is instantaneously consumed by tissue cells such that temporal lags from this process will introduce errors into calculated CMR_{O2} estimates over transition periods. To directly measure oxidative metabolism changes in blood or tissue oxygen produced by increases in neural activity, pharmacological agents have been used to suppress or reduce evoked changes in CBF (Fukuda *et al*, 2006; Nagaoka *et al*, 2006; Masamoto *et al*, 2008). These studies found that the calculated changes in CMR_{O2} are significantly slower than the evoked neural activity and CBF response, taking over 10 seconds to peak with sustained stimulation (Fukuda *et al*, 2006; Nagaoka *et al*, 2006; Masamoto *et al*, 2008; Vazquez *et al*, 2008; Offenhauser *et al*, 2005; Zappe *et al*, 2008). These relatively slow temporal changes in CMR_{O2} may be explained by the astrocyte-neuron-lactate-shuttle hypothesis (reviews in Pellerin *et al*, 2007 and Hertz, 2004), in which lactate is produced by increased glycolysis in astrocytes and then it becomes the primary substrate for oxidative metabolism in neurons. Another possibility for the relatively slow changes in CMR_{O2} may involve temporal latencies between mitochondria oxygen consumption and blood oxygen supply. Therefore, direct measurements of the tissue's mitochondria oxidative metabolic rate are essential to understand the dynamics of CMR_{O2} and how it impacts the oxygenation of blood and tissue.

This work consists of two aims: (1) to examine the temporal and spatial evolution of activation-evoked increases in CMR_{O2} as it originates in tissue cells and modulates the oxygen tension of tissue and also the oxygenation of blood, and (2) to examine the relationship between neural activity and oxidative metabolism. To accomplish these goals, neural activity, flavoprotein autofluorescence imaging (FAI), tissue oxygen tension (P_{O2}), and blood oxygenation-sensitive optical imaging of intrinsic signal (OIS, at a wavelength of 620 nm) were measured under a suppressed-CBF response condition. The imaging of tissue flavoprotein autofluorescence has been recently implemented to capture the changes in mitochondrial oxidative metabolism in the brain (Chance, 1968; Hassinen and Chance, 1968; Huang *et al*, 2002; Shibuki *et al*, 2003; Reinert *et al*, 2004; Weber *et al*, 2004; Tohmi *et al*, 2006; Husson *et al*, 2007; L'Heureux *et al*, 2009; Sirotin and Das, 2010) and is central to this work.

Materials and methods

Animal Preparation

Nine male Sprague-Dawley rats (200 to 500 g) were used in this work following an experimental protocol approved by the University of Pittsburgh Institutional Animal Care and Use Committee in accordance with the standards for humane animal care and use as set by the Animal Welfare Act and the National Institutes of Health Guide for the Care and Use of Laboratory Animals. The animals were initially anesthetized using isoflurane (5% for induction and 2% for surgery) in oxygen-enriched air or N_2O (30% to 50% inspired O_2) for intubation and placement of catheters in the femoral artery and femoral vein. The respiration rate and volume were controlled using a ventilator (TOPO; Kent Scientific, Torrington, CT, USA). After surgery, the animals were placed in a stereotaxic frame (Narishige, Tokyo, Japan) and the skull was exposed over the somato-sensory area. A well was made using dental acrylic surrounding an area 5 mm × 7 mm on the left side of the skull, centered 3.5 mm lateral and 1.5 mm rostral from Bregma. The skull in this area was then removed using a dental drill and cerebrospinal fluid was released around the cisterna magna area to minimize herniation. The dura mater was resected and the well area was then filled with 1% agarose gel at body temperature. Two needle electrodes were placed in the right forepaw between digits 2 and 4 for electrical stimulation. The anesthesia and breathing mixture were then modified to isoflurane (1.0% to 1.4%) in oxygen-enriched air (30% inspired O_2) for experimental recording. Rectal temperature was maintained at 37°C throughout with a DC temperature control module (40-90-8C; FHC Inc., Bowdoinham, ME, USA). Arterial blood sampling was periodically performed to measure systemic arterial blood oxygen tension (Pa_{O_2}), arterial carbon dioxide tension (Pa_{CO_2}), pH, hemoglobin concentration ([Hb]), and hematocrit (Hct) using a blood gas analyzer (Stat Profile, Nova Medical Corp., Waltham, MA, USA). The mean arterial blood pressure (MABP), respiration rate, heart rate, rectal temperature, end-tidal CO_2 tension, and isoflurane level were monitored and recorded using a polygraph data acquisition software (Acknowledge, Biopac Systems Inc., Goleta, CA, USA).

Experimental Conditions

Two experimental conditions were established: a control condition and a suppressed-CBF response condition. The control condition was the default condition established after the animal preparation was completed, in which evoked neural activation elicits CBF, cerebral blood volume (CBV), and CMR_{O2} responses (Figure 1). Experiments were performed under this condition to map the forelimb area in the somato-sensory cortex for probe and electrode placement. Since the vascular responses introduce unwanted contributions into the CMR_{O2} response, most of the data were

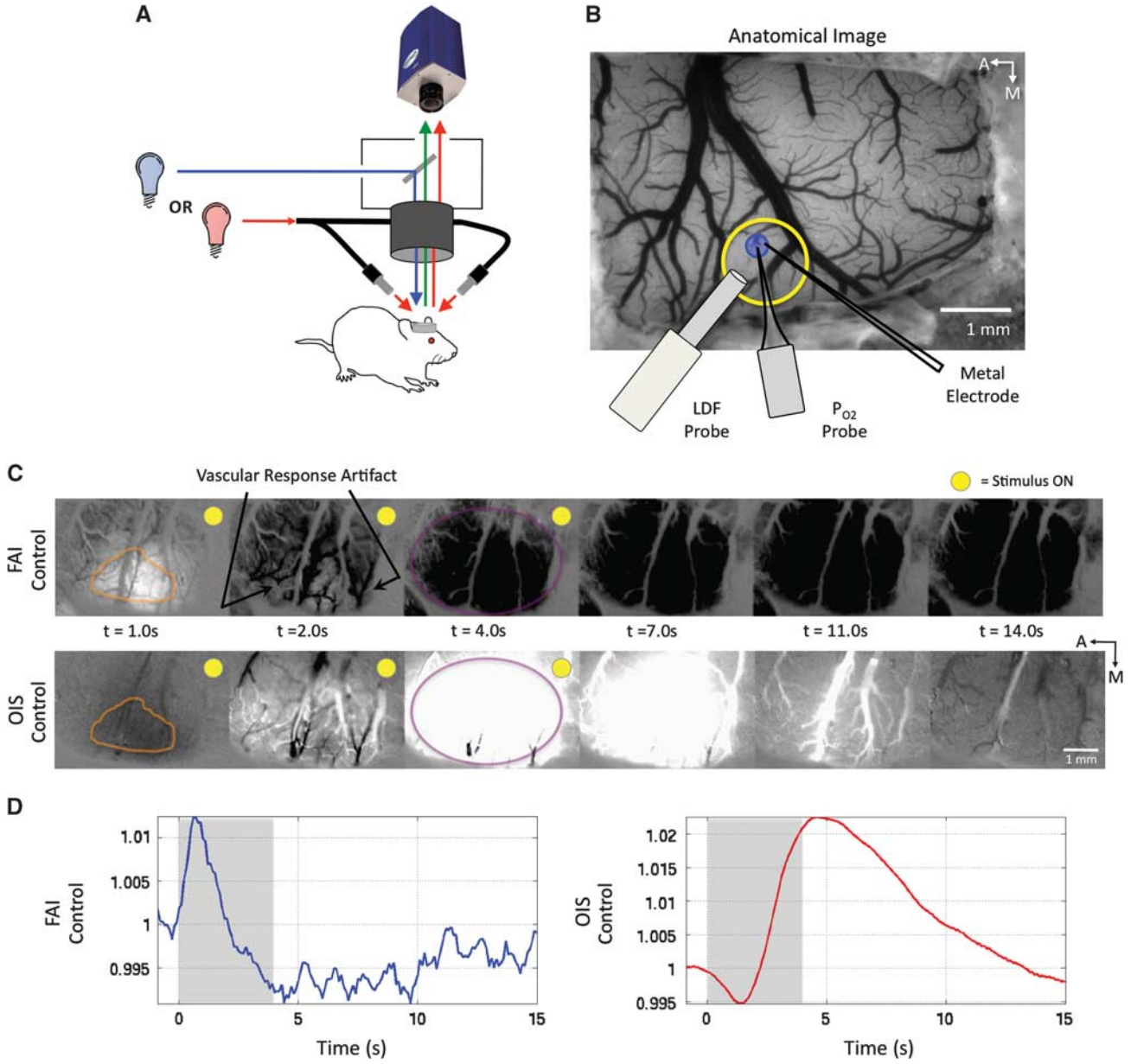

Figure 1 (**A**) Experimental set-up for imaging. An epifluorescence microscope was used to capture flavoprotein autofluorescence images (ex: 470 ± 20 nm, em: 525 ± 25 nm) or the changes in red light absorption (620 ± 10 nm) using obliquely transmitted red light for optical imaging of intrinsic signal. (**B**) Premapping experiments under control conditions (no vasodilator) using OIS and FAI were initially used to map the forelimb area in the somato-sensory cortex (outlined by the yellow circle) for placement of the LDF, tissue oxygen tension (P_{O2}), and metal electrode (sample subject shown). The circular region of interest (ROI) used to average FAI and OIS data, 200 μm in diameter and centered on the insertion point of the tissue P_{O2} probe, is shown in blue. (**C**) Expanded sample FAI (top panel) and OIS (bottom panel) response maps from a representative animal showing that within 1 second from stimulation onset, increases in FAI and decreases in OIS delineate well the forelimb area in the somato-sensory cortex (outlined in orange) due to increases in oxidative metabolism. More importantly, as the magnitude of the cerebral blood flow (CBF) and cerebral blood volume (CBV) responses increase shortly after (see two arrows), unwanted vascular contributions are introduced. It is also evident that the spatial extent of the CBF and CBV responses are larger (outlined in purple) than the responses observed right after stimulation onset. (**D**) Average time series obtained from the orange ROI show the temporal evolution of the FAI (left panel) and OIS (right panel) signals. The stimulation period is shaded in gray. FAI, flavoprotein autofluorescence imaging; OIS, optical imaging of intrinsic signal.

collected under the suppressed-CBF response condition, established by the administration of the vasodilatory agent sodium nitroprusside. The infusion of the agent was adjusted to target an MABP between 40 and 45 mm Hg over the course of the evoked stimulation experiments. The infusion of the agent was terminated after ~30 min. Before re-establishing this condition for additional experimental recordings, a resting period was used to restore the control

condition's baseline physiology (MABP and baseline laser Doppler flowmeter levels) for at least 1 hour. Then, the suppressed-CBF condition was re-established. In some cases, the re-administration of sodium nitroprusside did not reduce the MABP to the targeted range in a stable manner. In these cases, the administration of the agent was terminated and it was not re-attempted in these subjects. The overall average MABP during this condition was measured to be 47 ± 14 mm Hg and the overall average sodium nitroprusside infusion rate was 1.72 ± 0.92 mg/kg per hour ($n = 9$). All population data are reported as mean ± s.d. when provided, unless otherwise specified.

Experimental Design

Two short stimulation experiments were initially performed under control conditions to locate the activation area individually using FAI with excitation and emission wavelengths of 470 ± 20 and 525 ± 25 nm, respectively, and OIS at a wavelength of 620 ± 10 nm. At a wavelength of 620 nm, deoxygenated hemoglobin absorbs approximately $4\times$ more light than oxygenated hemoglobin (Horecker, 1943). Forepaw stimulation consisted of electrical pulses delivered using a pulse generator and isolator (Master 8 and ISO-Flex; A.M.P.I., Jerusalem, Israel) with the following parameters: 1.0 ms duration, 1.5 mA amplitude, a train of 48 pulses delivered at a frequency of 12 Hz, repeated 10 times every 16 seconds. These stimulation parameters were previously optimized to obtain robust responses under this experimental condition (Masamoto *et al*, 2007). The FAI and OIS data were used to map the forelimb area by subtracting the average image acquired 2 seconds before stimulation onset from the average image acquired over the first 2 seconds of the stimulation period. These activation maps were used to place a Clark-type oxygen sensor (Unisense, Aarhus, Denmark) with tip diameter of either 30 or 10 μm and a metal electrode with tip diameter of 5 μm (Carbostar-1; Kation Scientific, Inc., Minneapolis, MN, USA) at a depth of 300 μm over the hot spot of the activation area. Note that the sensitivity of the oxygen sensors spans at most $10\times$ their tip diameter (Fatt, 1976). In addition, a needle-type laser Doppler probe with tip diameter of 450 μm (operating wavelength of 780 nm; Perimed, Stockholm, Sweden) was positioned over the targeted location (Figure 1B). The spatial sensitivity of the LDF probe used spans a volume of $\sim 1\,mm^3$. After the probes were placed, at least 30 minutes elapsed before the first experiment was conducted.

To examine the temporal and spatial evolution of the CMR_{O2} changes under the suppressed-CBF response condition, the experimental stimulation paradigm consisted of 15 seconds of forelimb stimulation followed by 30 seconds of rest, repeated five times. Two stimulation frequencies were used, 3 and 12 Hz, with the same pulse parameters as above (1 ms pulses with amplitude of 1.5 mA). The FAI and OIS measurements were obtained in alternated manner until a minimum of 10 trials for each frequency (3 and 12 Hz) and imaging method (FAI and OIS) were obtained. Of the nine subjects tested, FAI and OIS data at a stimulation frequency of 3 Hz were obtained from nine and seven animals, respectively; while FAI and OIS data at a frequency of 12 Hz were obtained from a total of six and four animals, respectively. The stimulation parameters and experimental paradigm used were carefully selected to achieve the following: a stimulation period >10 seconds to reach a steady state for the oxidative metabolism signals, an intertrial period of 45 seconds to accommodate a relatively large number of trials and improve the signal-to-noise ratio, and alternating FAI and OIS experiments so as to reduce the continuous deposition of blue FAI excitation light over the course of the experiment.

Data Acquisition

The FAI and OIS data were acquired at 10 frames per second (f.p.s.) over the same field-of-view spanning an area $7.0. \times 5.2$ to $4.3 \times 3.3\,mm^2$ depending on the magnification using an epifluorescence macroscope (MVX-10; Olympus, Tokyo, Japan) and a digital cooled-CCD camera (CoolSnap HQ2; Photometrics, Princeton, NJ, USA). For FAI, a mercury lamp light source coupled to a low-noise power supply (Opti-quip, Highland Mills, NY, USA) was used. The camera's exposure time was set to 100 ms with a bin factor of 4 to increase signal-to-noise for an effective pixel resolution between 12.8 and 20.4 μm. For OIS, oblique light guides transmitting filtered red light connected to a halogen light source (Thermo-Oriel, Stratford, CT, USA) were used for illumination and a matching barrier filter was placed before the camera (see Figure 1A). The exposure time was decreased to 20 ms with a bin factor of 2 while the frame rate was maintained at 10 f.p.s. Laser Doppler flowmetry and tissue P_{O2} data were recorded using the polygraph data acquisition software during all experiments at a frequency of 1 kHz. In addition, electrophysiological recording of multi-unit spiking activity (300 Hz to 8.8 kHz) was recorded using the metal electrode at a frequency of 20 kHz (MAP, Plexon, Inc., Dallas, TX, USA) in six of the nine animals tested.

Data Analysis

All the data were analyzed using Matlab (Mathworks, Natick, MA, USA). After all the experimental data were collected, the FAI and OIS data were temporally linearly detrended to filter out potential fluctuations in the light source using a reference time series extracted from a region of interest (ROI) positioned over the skull or dental acrylic. Multi-unit activity (MUA) was quantified by counting the number of outward zero-crossings exceeding a threshold of $2.5\times$ the standard deviation of pre-stimulation baseline data over 50 ms temporal bins. Neural activity data spanning a window of -1 to 4 ms from each evoked stimulus onset (1 ms electrical pulse) were discarded to avoid the inclusion of stimulation artifacts. The FAI, OIS, P_{O2}, LDF, and MUA data of each subject from the various trials were then averaged. The P_{O2} data were corrected for measurement lags (measured to be 0.6 seconds to 90% of the final amplitude for the oxygen sensors used) by

deconvolution with an exponential function. The resulting data were then low-pass filtered with a 5-Hz rectangular cutoff. The tissue P_{O2} and LDF data were then baseline normalized by their average value over 5 seconds before stimulation onset.

Temporal Analysis

To compare the tissue P_{O2} with the FAI and OIS responses, a circular ROI 200 μm in diameter was defined, centered over the penetration point of the P_{O2} probe, excluding the P_{O2} probe and the metal electrode. The FAI and OIS time series over the ROI were extracted from the raw data, the trials were averaged and then normalized by their average baseline intensity over the 5-second period before stimulation onset for each subject. Measurements of the time-to-10% and time-to-90% peak change during and after the stimulation period were measured from the averaged data to examine the temporal evolution of the oxidative metabolism changes. The peak change was defined as the average signal value over a 3-second period centered on the peak value of the data. In addition, a first-order model (Equation (1)) was used to fit the FAI, tissue P_{O2} and OIS data using the MUA envelope as the input (U) to determine the time constant of these responses (τ).

$$\frac{dy}{dt} = \frac{1}{\tau}(U(t) - \alpha y(t)) \quad (1)$$

The scaling (α) and time-constant (τ) parameters were determined using a least-squares minimization routine implemented in Matlab. The tissue P_{O2} and OIS data were then fit again using the first-order model and the fit FAI response as the input $U(t)$ to determine the tissue P_{O2} and OIS response time constants relative to FAI signal changes.

Spatial Analysis

To investigate the spatial evolution of the FAI and OIS responses, activation maps were calculated over the stimulation period averaged to a temporal resolution of 1 second for each subject (15 images in total). The maps were smoothed using a Gaussian filter (two pixels wide for FAI and four pixels wide for OIS) and the number of pixels over a threshold of $>25\%$ the peak maximum and minimum changes of each FAI and OIS activation map, respectively, was counted and converted to area (in mm^2). The mean diameter of the activation area was then calculated and plotted as a function of time assuming that it is roughly circular in shape. In addition, the centroid of the activation area was determined for each subject using the activation map weighted by the intensity of each pixel location (e.g., $C = \Sigma_n\ x_n I_n / \Sigma_n\ I_n$ where C is the centroid location along coordinate x with intensity I). The distance between the FAI and OIS centroids was calculated. Finally, temporal changes in FAI and OIS were obtained by averaging the intensities of all pixels over a threshold of $>25\%$ its peak magnitude change over three exclusive circular areas centered at the activation centroid and extending 200 μm (ROI 1), 600 μm (ROI 2), and >600 μm (ROI 3) in diameter.

Neuronal Activity Analysis

Finally, to investigate the correlation between evoked neural activity and the changes in oxidative metabolism, the integral and peak changes in MUA were compared with the integral and peak changes in FAI, tissue P_{O2}, and OIS. The average data from each subject for both stimulation frequencies, 3 and 12 Hz, were considered for this analysis. To assess significance, the correlation coefficients were transformed to t-values and one-sided t-tests were performed.

Results

The physiological condition of all the subjects was maintained within appropriate physiological levels after surgical preparation (Table 1). Preliminary OIS and FAI experiments were then performed to map the forelimb area for placement of the tissue P_{O2} probe and a metal electrode close together at the center of the activation area while avoiding visible surface vessels (Figure 1). Examination of the OIS and FAI maps beyond the first 2 seconds of the stimulation period shows significant contributions of the CBF response to the OIS and FAI data. In the OIS data, the CBF response contribution is manifested as the large increase in blood oxygenation (brightening) that takes place several seconds after stimulation onset and lasts for $\sim$12 seconds (Figures 1C and 1D). In the FAI data, the CBF response contribution is manifested as the large darkening of the FAI response due to increases in CBV that absorb the FAI-emitted light. These data show the need to suppress the CBF response and its associated CBV response to investigate the spatio-temporal properties of CMR_{O2} using FAI, tissue P_{O2}, and OIS. Therefore, sodium nitroprusside was administered to suppress evoked CBF and CBV responses without impacting neural activity as demonstrated previously (Fukuda *et al*, 2006; Masamoto *et al*, 2008) and maximally sensitize the measurements to the functional changes in oxidative metabolism.

Under the suppressed-CBF response condition, evoked neural and metabolic responses to electrical

Table 1 Physiological parameters measured at the femoral artery before establishing the suppressed-CBF response condition

Parameter	*Value*
pH	7.44 ± 0.03
Pa_{CO_2}	39.2 ± 4.2 mm Hg
Pa_{O_2}	121.9 ± 17.4 mm Hg
[Hb]	12.9 ± 0.8 g/dL
Hct	38.8 ± 2.5%
MABP	86 ± 17 mm Hg

Abbreviations: CBF, cerebral blood flow; [Hb], hemoglobin concentration; Hct, hematocrit; MABP, mean arterial blood pressure; Pa_{CO_2}, arterial blood carbon dioxide tension; Pa_{O_2}, arterial blood oxygen tension.
These parameters were observed to be within normal physiological levels in all subjects ($n = 9$).

forelimb stimuli were recorded. Robust and significant increases in MUA were observed with stimulation (Figure 2A; Supplementary Figure S1A), while the changes in CBF, monitored using LDF, were largely suppressed, showing average peak increases in CBF of $<3\%$ (Figure 2B; Supplementary Figure S1B). It is worth noting that the magnitude of stimulation-evoked CBF responses under control conditions is typically between 30% and 50% (Masamoto *et al*, 2007; Vazquez *et al*, 2008). The increases in MUA were observed to quickly peak and then decrease by 47% and 92% by the end of the stimulation period for stimulation frequencies of 3 and 12 Hz, respectively (Figure 2A; Supplementary Figure S1A).

Temporal Changes in Oxidative Metabolism Measured by Flavoprotein Autofluorescence Imaging, Tissue Oxygen Tension, and Optical Imaging of Intrinsic Signal

To investigate the temporal evolution of the changes in oxidative metabolism, a circular ROI, 200 μm in diameter and centered on the insertion point of the P_{O2} probe, was selected to average the FAI and OIS data (blue circle in Figure 1B). The increases in tissue mitochondria oxidative metabolism measured using FAI were observed to resemble the temporal envelope of the MUA during the stimulation period, quickly increasing with stimulation onset, and then slightly decreasing during the rest of the stimulation period (Figure 2C; Supplementary Figure S1C). Average peak increases in the FAI signal of $0.64 \pm 0.28\%$ ($n=9$) were observed for 3 Hz stimulation (see individual time courses in Supplementary Figure S2) and $0.48 \pm 0.44\%$ ($n=6$) for 12 Hz stimulation, which decreased by $\sim 40\%$ and $\sim 100\%$ by the end of the stimulation period, respectively. After stimulation offset, the FAI signal was observed to decrease below baseline, reaching a minimum 5 to 20 seconds after stimulation offset and then the signal returned to baseline. The corresponding activation-evoked changes in tissue P_{O2} were monophasic and negative, as expected since the CBF response was mostly suppressed, with average peak decreases of $-2.5 \pm 2.2\%$ ($n=16$) for 3 Hz stimulation and $-4.4 \pm 3.2\%$ ($n=10$) for 12 Hz stimulation (Figure 2D; Supplementary Figure S1D). The corresponding changes in blood oxygenation measured by OIS were also monophasic and negative, as expected, and showed average peak decreases in the OIS signal of $-0.13 \pm 0.072\%$ ($n=7$) for 3 Hz stimulation and $-0.19 \pm 0.13\%$ ($n=4$) for 12 Hz stimulation (Figure 2E; Supplementary Figure S1E).

The temporal characteristics of the oxidative metabolism responses measured by FAI, tissue P_{O2}, and OIS were quantified by measurements of the time-to-10% peak and time-to-90% peak from the average data over the onset and offset response periods (Table 2). In addition, a first-order model (Equation (1)) was fit to the average FAI, tissue P_{O2}, and OIS data using the envelope of the average MUA as the input to obtain time constants (τ) for these responses and further assess the general temporal properties of this evolution (Table 2; Figure 2, black lines). To investigate the time constant between CMR_{O2} changes at the cellular level and those at the tissue and blood oxygenation levels, the first-order model was individually fit to the tissue P_{O2} and OIS responses using the fit to the FAI data as the input *U(t)* (Table 2; Figures 2D and 2E, black dashed lines). This model captured the general dynamics of the responses although it was not designed to fit the post-stimulation undershoot of the FAI data. Altogether, these results show a fast onset in tissue mitochondria oxidative metabolism, followed by a slower consumption of the overall tissue oxygen and a demand for blood oxygen shortly after.

Spatial Changes in Oxidative Metabolism Measured by Flavoprotein Autofluorescence Imaging and Optical Imaging of Intrinsic Signal

The spatial dynamics of the oxidative metabolism responses were examined using the FAI and OIS data at a stimulation frequency of 3 Hz to generate baseline-subtracted maps over the course of the experiment trial. A map sequence showing the features of the metabolic changes from tissue (FAI) and blood (OIS) signals from one subject is presented in Figure 3A. The first frame shows the baseline image used for subtraction, followed by the sequence of subtracted images during the stimulation period (marked with a

Figure 2 Average evoked changes in (**A**) multi-unit neural activity (ΔMUA; units of spikes/seconds, $n=6$; stimulation period indicated by the shaded area), (**B**) cerebral blood flow (CBF) measured using LDF (%, $n=9$), (**C**) the tissue mitochondria oxidative rate measured using FAI (%, $n=9$), (**D**) tissue oxygen tension (P_{O2}) (%, $n=9$), and (**E**) blood oxygenation measured using OIS (%, $n=7$) elicited by somato-sensory stimulation at a frequency of 3 Hz for 15 seconds under the established suppressed-CBF response condition. The data in (**A**) and (**B**) show that robust increases in neural activity were elicited while the CBF response was mostly suppressed (average peak increase of 2.5% and time-to-90% peak of 6.3 seconds). The inset in (**C**) shows the envelope of the average multi-unit activity shown in Figure 2A. The error bars indicate the standard error. Note that the increases in FAI were rapid compared to the decreases in tissue P_{O2} or blood oxygenation which reached peak at the end of the stimulation period. A first-order model was then fit to the FAI, tissue P_{O2}, and OIS data using the envelope of the multiunit activity as input (black solid line in **C**–**E**). In addition, the tissue P_{O2} and OIS data were fit using this model along with the fit of the FAI data (black line in **C**) as their input (resulting fits shown as black dashed lines in **D** and **E**). The time constants of these fits are reported in Table 2. FAI, flavoprotein autofluorescence imaging; OIS, optical imaging of intrinsic signal.

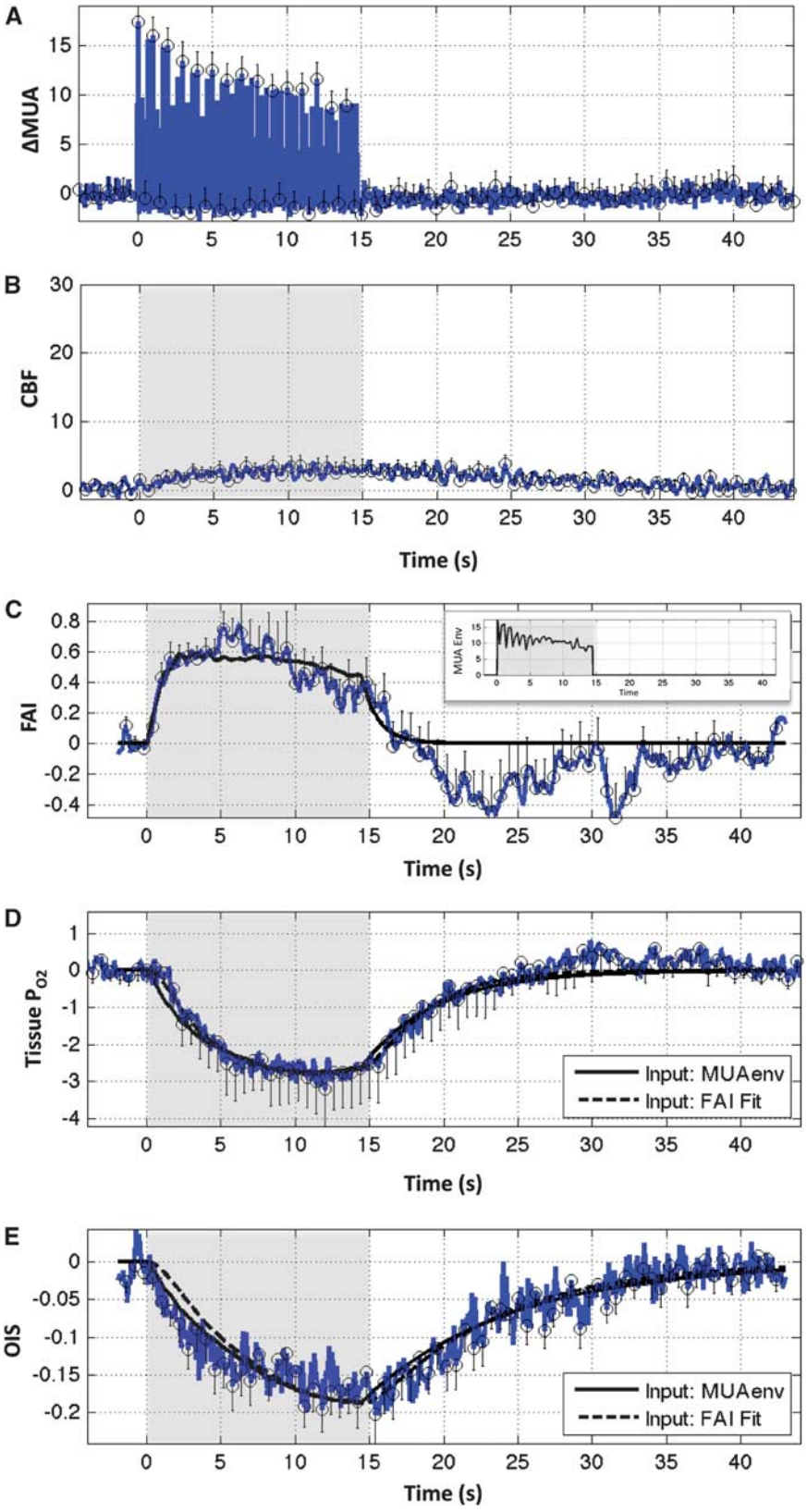

yellow circle) and after the stimulation period. The changes in the tissue mitochondria oxidative rate captured by FAI first showed a fast increase in signal (brightening) and spatial extent with stimulation onset that reached peak in several seconds. The signal was then observed to gradually decrease in both intensity and extent during the rest of the stimulation period in similar manner to its temporal

Table 2 Average onset time-to-10% peak (t_{10}, in seconds), onset time-to-90% peak (t_{90}, in seconds), offset t_{10} (in seconds), offset t_{90} (in seconds), peak amplitude and first-order time constant (τ, in seconds) for the FAI, tissue P_{O2}, and OIS responses to 3 and 12 Hz stimulation frequencies

Frequency	*Data*	*Onset t_{10}*	*Onset t_{90}*	*Offset t_{10}*	*Offset t_{90}*	*Peak*	*τ*
3 Hz	FAI	0.2	2.2	N/A	1.3	0.64%	1.1
	Tissue P_{O2}	0.3	5.9	0.1	7.5	−2.5%	4.9 (3.6)
	OIS	0.4	5.3	1.3	16.4	−0.13%	10.0 (8.4)
12 Hz	FAI	0.0	0.6	N/A	0.2	0.48%	0.7
	Tissue P_{O2}	0.1	3.2	0.0	7.7	−4.4%	5.2 (4.3)
	OIS	0.2	3.8	0.4	12.7	−0.19%	10.2 (9.1)

Abbreviations: FAI, flavoprotein autofluorescence imaging; MUA, multi-unit activity; OIS, optical imaging of intrinsic signal; P_{O2}, tissue oxygen tension.
The estimated time constants were determined from fits to the data using a first-order model and the envelope of the changes in MUA (τ) elicited by stimulation as input. The fitted FAI response was also used as the input to the P_{O2} and OIS responses and the resulting time constant is reported in parenthesis.

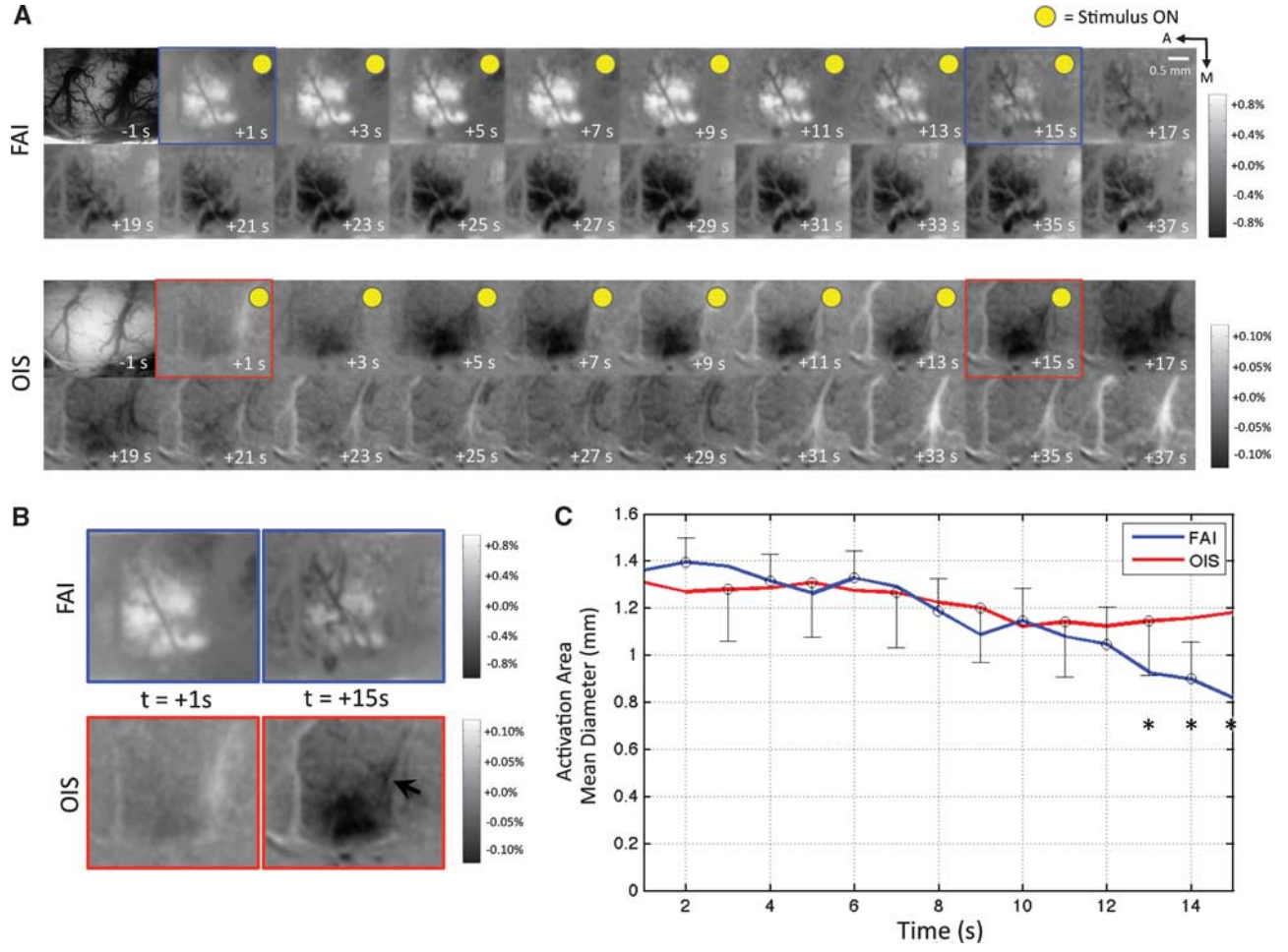

Figure 3 Spatial cerebral metabolic rate of oxygen consumption (CMR_{O2}) responses captured by FAI and OIS to forelimb stimulation at a frequency of 3 Hz for 15 seconds under suppressed-cerebral blood flow (CBF) response conditions. (**A**) Baseline-subtracted FAI (top) and OIS (bottom) map sequence obtained every 2 seconds over the course of an experiment (average time shown at the bottom of each image). The first frame in each sequence ($t = -1$ second) consists of the FAI and OIS baseline image. Frames where the stimulus was present are marked with a yellow circle at the top-right corner of each image. (**B**) Two enlarged FAI and OIS maps from temporal frames $t = +1$ (immediately after stimulation offset) and $t = +15$ (end of stimulation period) are shown to highlight the differences between FAI and OIS as a function of time presented in (**A**). The arrow in the bottom-right OIS frame shows evident vascular drainage signal contributions. (**C**) Average diameter of the activated area as a function of time as captured by FAI (blue line) and OIS (red line). The error bars indicate the standard error ($n = 9$ for FAI, $n = 7$ for OIS). The sizes of the activated area calculated using both FAI and OIS data were in good agreement. Statistical analyses were performed by comparing the data with that from the first second of the stimulation period (* indicates significant differences with $P < 0.05$). FAI, flavoprotein autofluorescence imaging; OIS, optical imaging of intrinsic signal.

profile in Figure 2. After stimulation offset, the signal decrease (darkening) was observed to span an area similar to that during the stimulation period. However, the oxidative metabolism changes in blood oxygenation captured by OIS were monophasic, showing a gradual decrease in signal that appears to increase in spatial extent during the stimulation period, and a similar gradual return to baseline after stimulation offset. To further capture this difference between CMR_{O2}-driven changes in tissue and blood, expanded FAI and OIS maps from the beginning and end of the stimulation period are shown in Figure 3B. Note that vascular artifacts are evident in the OIS maps (see black arrow) but not in the FAI maps.

To quantify the size of the activation area, the average diameter was calculated over 1 second intervals during the stimulation period using a threshold of $>25\%$ of their peak signal change in each map (Figure 3C). The average diameters of the FAI and OIS activation areas were 1.34 ± 0.31 mm ($n=9$) and 1.29 ± 0.57 mm ($n=7$), respectively, over the first 5 seconds of the stimulation period. The centroids of the FAI and OIS activation areas were found to be similar, differing in distance by only 52 μm (± 34 μm, $n=7$). The spatial extent of the FAI and OIS maps was relatively stable during most of the stimulation period, especially for the OIS data, but they were observed to decrease on average by 38.9% and 8.5%, respectively, by the end of the stimulation period. To further investigate the spatio-temporal properties of oxidative metabolism, the average FAI and OIS time courses were obtained from three exclusive circular ROIs positioned at the centroid of activity and extending 200, 600, and >600 μm in diameter (Figure 4). As expected, the signal magnitude decreased as the distance from the centroid increased. In addition, the ratio of the FAI and OIS time courses as a function of distance was not different, indicating that the spatial relationship between the mitochondria oxidative rate and blood oxygenation is similar.

Neural Activity Analysis

To examine the correlation between oxidative metabolism responses and neural activity, comparisons between the average MUA, FAI, tissue P_{O2}, and OIS signals were made across subjects and the two stimulation frequencies used (Figure 5). In general, MUA was found to be correlated with oxidative metabolism responses. Significant correlations were found between the peak MUA and the peak FAI signal ($r=0.77$, $n=12$, $P<0.01$), while a weaker correlation was found between the area of the MUA and the area of the FAI signal during the stimulation period ($r=0.53$, $n=12$, $P<0.1$). Similarly, significant relationships were found for the changes in tissue P_{O2} ($r=0.49$, $n=19$, $P<0.05$ for peak MUA versus peak tissue P_{O2}; $r=0.84$, $n=19$, $P<0.001$ for MUA area versus tissue P_{O2} area), and similar but weaker relationships were found for the OIS data ($r=0.64$, $n=7$, $P<0.15$ for MUA area versus OIS area).

Discussion

This work investigated the properties of the evolution of activation-evoked increases in CMR_{O2} elicited by somato-sensory stimulation, as it originates in tissue mitochondria and modulates the oxygen tension of tissue and blood oxygenation. Temporally, a fast increase in the tissue's mitochondria oxidative metabolic rate was observed with evoked stimulation using FAI, taking as little as 0.6 seconds to reach 90% peak amplitude (for 12 Hz stimulation, or 2.2 seconds for 3 Hz stimulation). CMR_{O2}-driven changes in the tissue P_{O2} and blood oxygenation followed shortly after, but the magnitude of these changes increased slowly, both reaching peak near the end of the stimulation period. Spatially, the changes in mitochondrial oxidative metabolism and blood oxygenation were similar, quickly spanning a relatively large area with stimulation onset. Finally, the increases in mitochondria oxidative metabolism were well correlated with the evoked neural activity as represented by multi-unit spiking activity. To date, this is the first known study to report the spatial and temporal dynamics of mitochondria oxidative metabolism and its impact on tissue and blood oxygenation in the cortex *in vivo*. In addition, a simple model was used to determine the temporal relationship between the changes in neural activity, tissue mitochondria CMR_{O2}, and the CMR_{O2}-driven changes in tissue and blood oxygenation. It should be noted that under suppressed-CBF conditions, the temporal changes in OIS closely resemble those of blood oxygen level-dependent (BOLD) functional magnetic resonance imaging (fMRI) (Fukuda *et al*, 2006 versus Nagaoka *et al*, 2006), such that the OIS findings reported in this work are directly applicable to BOLD-based CMR_{O2} studies.

Temporal Cerebral Metabolic Rate of Oxygen Consumption Responses

The temporal changes in mitochondrial oxidative metabolism were found to be relatively fast and resembled the temporal envelope of the evoked neural activity. Fast increases in FAI signal were observed in the studies performed for this work and also in other similar studies in the literature (Shibuki *et al*, 2003; Reinert *et al*, 2004; Weber *et al*, 2004; Tohmi *et al*, 2006; Husson *et al*, 2007; L'Heureux *et al*, 2009; Sirotin and Das, 2010; Vazquez *et al*, 2010). In addition, *in vitro* studies of nicotinamide adenine dinucleotide also showed a fast, transient increase in oxidative metabolism, followed by a larger increase in glycolysis (Kasischke *et al*, 2004). Nicotinamide adenine dinucleotide studies can be sensitive to both glycolysis and the tricarboxylic acid

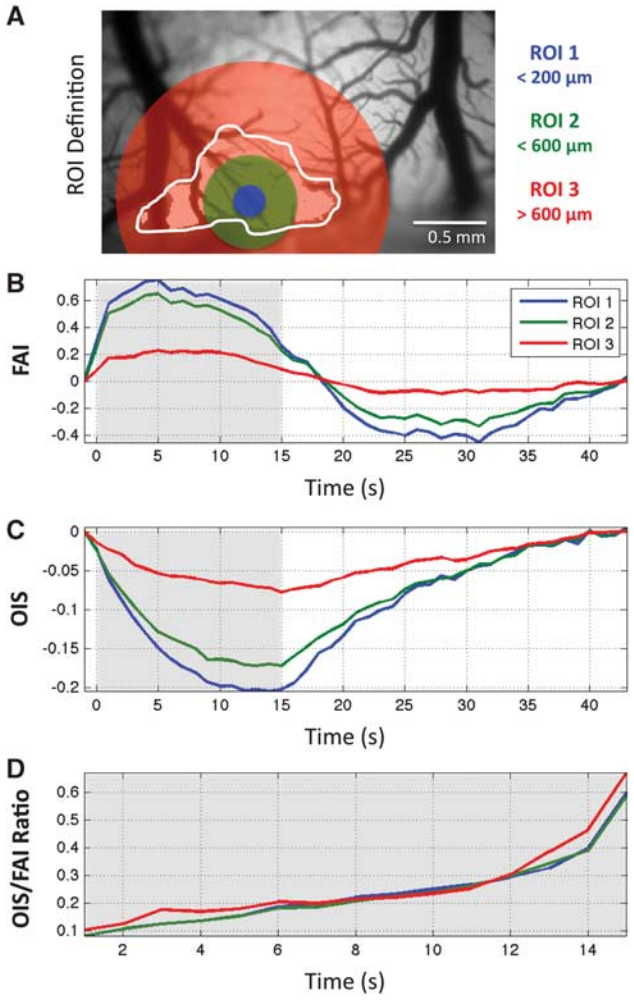

Figure 4 Average FAI (**B**) and OIS (**C**) signal changes over three different regions of interest (ROIs) (**A**) which were selected as the intersection between the average activation map calculated for each subject using a threshold of $>25\%$ the peak magnitude change and exclusive co-centric rings with diameters between 0 and 200 μm (ROI 1), 200 and 600 μm (ROI 2), and 600 and 2,000 μm (ROI 3). (**D**) Ratio of the OIS and FAI signal changes during the stimulation period for the three selected ROIs. The average FAI and OIS spatio-temporal signal changes were very similar during the stimulation period indicating that both methods outline very similar spatial changes in cerebral metabolic rate of oxygen consumption (CMR_{O2}) under suppressed-CBF conditions. CBF, cerebral blood flow; FAI, flavoprotein autofluorescence imaging; OIS, optical imaging of intrinsic signal.

cycle because it participates in both of these metabolic cascades (glycolysis in the cell cytoplasm and the tricarboxylic acid cycle in the mitochondria). However, $FADH_2$ redox takes place in the mitochondria of cells, making the changes in FAI signal specific to changes in the tricarboxylic acid cycle rate. While most of the FAD fluorescence stems from the activity of Complex II of the electron transport chain and lipoamide dehydrogenase complexes (e.g., pyruvate dehydrogenase complex), it is important to note that FAD is also reduced in a step within the tricarboxylic acid cycle, such that FAI reflects the oxidative rate as long as the oxidation of $FADH_2$ exceeds FAD reduction. If the oxidation of $FADH_2$ and reduction of FAD balance, then FAI would underestimate the changes in the oxidative rate. Since the changes in FAI were observed to be positive throughout the stimulation period in similar manner to the neural activity, it will be assumed in this work that the oxidation of $FADH_2$ exceeds FAD reduction and that FAI is indicative of dynamic oxidative metabolism.

The fast increases in tissue mitochondria CMR_{O2} measured by FAI were described by a time constant of $\sim$1 second and it might describe the process behind the astrocyte-neuron lactate shuttle hypothesis if it occurs within this temporal frame. The increased consumption of oxygen in tissue cells then draws oxygen from tissue and also from blood, but at a slower rate. Blood oxygenation data obtained using fMRI (BOLD) and OIS under the same experimental condition used in this work (suppressed-CBF) have also shown relatively slow temporal changes to somato-sensory stimulation in rats and visual stimulation in cats (Fukuda *et al*, 2006; Nagaoka *et al*, 2006; Masamoto *et al*, 2008). Collectively, the findings presented indicate that the consumption of oxygen in cellular mitochondria is significantly faster than the oxygen supply from tissue and blood with an average time constant of 3.9 and 8.7 seconds, respectively. This is most likely due to two factors: (1) differences between the sizes of the oxygen demand (mitochondria) and tissue oxygen supply pools (intracellular as well as extracellular oxygen in tissue), and (2) diffusion lag between nearby vessels and active cells. It is interesting to note that if the calculated time constants between the changes in the tissue mitochondria oxidative rate and the changes in tissue P_{O2} and blood oxygenation reflect oxygen diffusion time, then mean diffusion distances of 90 and 135 μm would be estimated ($D_{O2} = 1 \times 10^{-5}$ cm^2/s), which are larger than the mean intercapillary distance (Pawlik *et al*, 1981) and do not fully account for diffusion lag between active cells and nearby vessels.

After stimulation offset, the FAI signal was observed to decrease below baseline (darkening). The spatial extent of this portion of the FAI response was found to be similar to that of the FAI signal increase (brightening) during stimulation, differing in diameter by $\sim$4%. The mechanism behind the darkening of the FAI response is still unclear and it was not systematically investigated in this work. In a report by Reinert *et al* (2004), decreases in FAI were attributed not only to increases in CBF and CBV (which were minimal in this study) but also by the reduction of flavoproteins associated with an increase in mitochondrial reducing agents (e.g., nicotinamide adenine dinucleotide). Although this mechanism is likely responsible for the decrease in the FAI signal after stimulation, no pharmacological manipulations were performed in this work to assess its source.

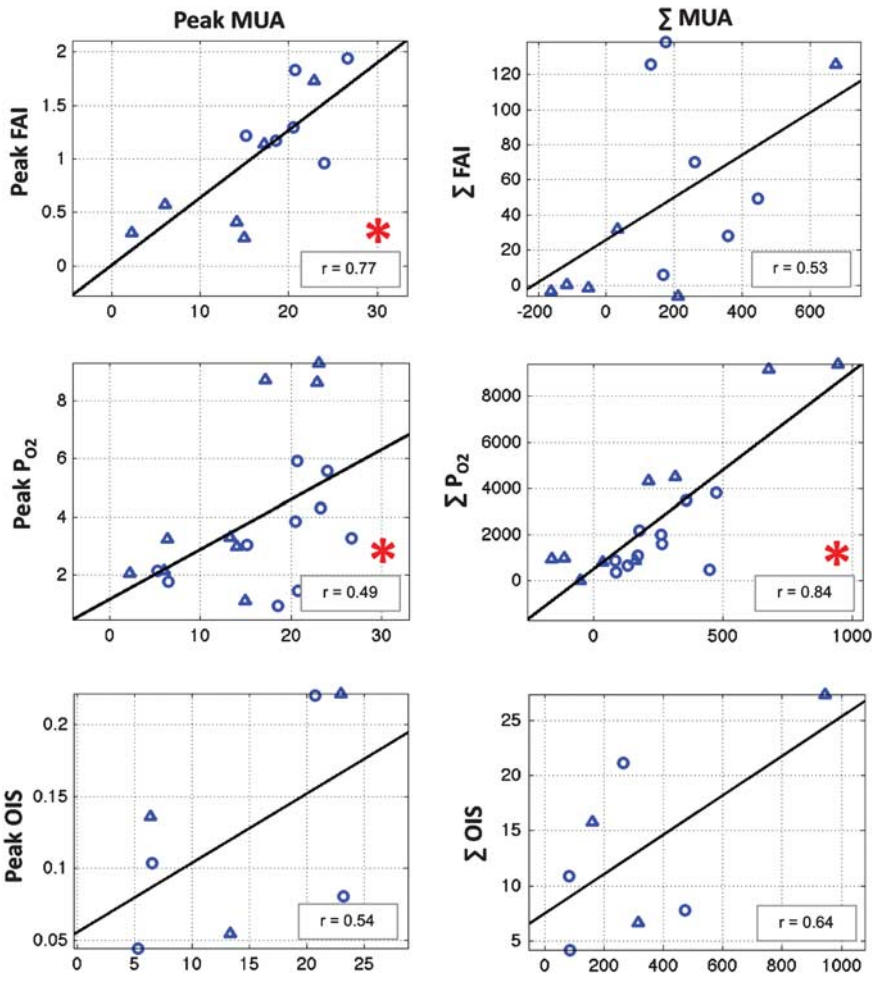

Figure 5 Correlation between the cerebral metabolic rate of oxygen consumption (CMR_{O2})-driven changes measured by FAI, tissue oxygen tension (P_{O2}), OIS and their corresponding evoked neural activity. Averaged data from each subject and for each stimulation frequency tested (3 Hz data shown as circles and 12 Hz data shown as triangles) were included in this analysis. The relationship between FAI, tissue P_{O2}, OIS, and multi-unit activity (MUA) was then determined considering the peak change of each measurement over baseline as well as the integral of the evoked changes over baseline. The polarity of the P_{O2} and OIS signal changes was reversed for this analysis. Significant relationships ($P < 0.05$) are indicated with a red asterisk (*) over the figure legend. The changes in FAI and P_{O2}, and P_{O2} and OIS were found to be significantly correlated ($r = 0.60$, $P < 0.02$ and $r = 0.62$, $P < 0.05$ for their peak magnitude changes over the stimulation period, respectively). FAI, flavoprotein autofluorescence imaging; OIS, optical imaging of intrinsic signal.

Further systematic studies are necessary to determine the source of the FAI response darkening.

Spatial Cerebral Metabolic Rate of Oxygen Consumption Responses

The spatial changes in oxidative metabolism measured using FAI were found to span an area with diameter of 1.34 ± 0.31 mm. Reports of the size of the entire rat forelimb somato-sensory area performed using histochemistry and electrophysiology have found that it spans a diameter between 1.4 and 1.7 mm (Riddle and Purves, 1995; Coq and Xerri, 1999), which is slightly larger but within the error of the FAI and OIS measurements. Residual size differences are possibly due to activating a subset of the forelimb nerve fibers (electrical leads were placed between digits 2 and 4 of the forelimb) and selection of the intensity threshold. Further, the size of the changes in oxidative metabolism measured by FAI was very similar to those measured by OIS showing that although the changes in blood oxygenation were temporally slower, they closely match the spatial extent of the changes in oxidative rate. Although decreases in the average activation area of FAI and OIS were observed, only the decreases in the FAI maps near the end of the stimulation period were found to be significant. This may be due to the reduction in MUA during the end of the stimulation period and the onset of the negative phase of the FAI signal. Interestingly, the apparent slow increase in the spatial extent of the OIS data was due to the slow temporal dynamics of the changes in blood

oxygenation. A pixelwise correlation analysis of the changes in FAI and OIS signals performed over a common area showed significant relationships in most subjects, although evident deviations were observed in the OIS maps over vascular draining areas (evident in Figure 3). In general, the changes in oxidative metabolism have been reported to be better localized to the area of activity compared with hemodynamic changes (Husson *et al*, 2007; Sirotin and Das, 2010). For example, a study performed by Husson *et al* investigated the spatial properties of the changes in FAI signal compared with those of OIS for mapping columnar domains in the visual cortex and found that the FAI point spread function was sharper than that of OIS obtained with CBF contributions. Similar findings were also reported in the visual cortex of awake primates by Sirotin and Das. The OIS measurements obtained in our study under control conditions (no vasodilator) to map the forelimb area for placement of the tissue P_{O2} and metal electrodes consistently showed larger spatial hemodynamic responses compared with FAI and OIS with vasodilator (Figure 1 versus Figures 2 and 3), indicating that the area of activity delineated by changes in metabolism is better localized than that obtained from hemodynamic maps. In addition, the close similarity in the spatial extent of the CMR_{O2}-driven FAI and OIS signal changes (Figure 4) reinforces that the changes in blood oxygenation due to increases in CMR_{O2} are very well confined to the areas with increased oxidative demand.

Neuronal Activity

Finally, this study also investigated the relationship between the changes in oxidative metabolism and the changes in neuronal activity. Significant relationships between the increases in CMR_{O2} and MUA were found, especially when comparing the peak changes in CMR_{O2} as described by FAI, tissue P_{O2}, and OIS. The comparisons performed using the energy of the FAI, tissue P_{O2}, and OIS signals were weaker likely due to variability in the data, especially over temporal differences involving the decrease in FAI during the stimulation period (see Supplementary Figure S2).

Other studies have reported significant correlations between neural activity and CMR_{O2} (Smith *et al*, 2002; Thompson *et al*, 2003; Masamoto *et al*, 2008). A report by Thompson *et al* (2003) showed that the P_{O2} in visual cortex orientation domains decreased during preferred-orientation stimulation due to increases in spiking activity, but not during non-preferred orientation stimulation which do not elicit significant changes in spiking activity. This suggested that the functional CMR_{O2} response is sensitive to the spiking rate. Similarly, this study also found that activation-evoked changes in oxidative metabolism are well correlated with multi-unit spiking activity. In a previous study by Masamoto *et al* (2008), the intra-subject inter-trial relationship between field potential activity and CMR_{O2}-driven decreases in tissue P_{O2} and OIS was also found to be well correlated. Since MUA is closely related to field potential activity, particularly for stimuli that elicit robust spiking activity, the results presented support the notion that CMR_{O2} is strongly correlated with spiking activity and also with local field potential activity.

Implications

The findings reported in this work show that changes in oxidative metabolism alone evoked by increases in neuronal activity, whether measured by specific tissue signals or less directly by changes in blood oxygenation, are very well confined to the area of activity. In addition, indirect measurements of CMR_{O2} such as those obtained using blood oxygenation data do not directly reflect the dynamic changes in the mitochondrial metabolic rate; instead they more closely resemble the average changes in oxidative metabolism of the entire tissue pool. This lag between oxygen consumption at the cellular level and oxygen extracted from blood was found to be on the order of a few seconds, implying that the oxygen consumption and blood oxygen extraction process is not instantaneous, a common assumption used in the calculation of CMR_{O2} from hemodynamic data.

Two important implications for BOLD fMRI studies can be outlined. First, the CMR_{O2}-driven changes in blood oxygenation (OIS) after stimulation offset were observed to slowly return to baseline. This portion of the blood oxygenation response is a likely source for the post-stimulus undershoot commonly observed in BOLD fMRI data, supporting the notion that the BOLD post-stimulus undershoot partly reflects previous oxidative metabolism demands incurred by increased activity during the stimulation period. Second, the calculation of CMR_{O2} from hemodynamic data (CBF, CBV, and BOLD) is theoretically accurate over steady-state periods where oxygen demand matches oxygen supply; however, it is not accurate over transition periods. This assertion is evident in the CMR_{O2}-driven changes in OIS signal since its use for the calculation of the CMR_{O2} changes using typical steady-state models will yield CMR_{O2} changes with the same temporal profile as the OIS data (time constant of $\sim$10 seconds). To partly explain this temporal difference between tissue cellular CMR_{O2} and CMR_{O2}-driven blood oxygenation changes, relatively simple dynamic models can be used (Vazquez *et al*, 2008; Zheng *et al*, 2002; Huppert *et al*, 2009). However, these models are not sufficient to fully explain the observed temporal lag. The findings presented here can be used to develop more sophisticated oxygen transport models that better describe blood oxygen delivery and cellular oxygen consumption. Moreover, our findings can be used to adapt current models that quantify CMR_{O2} from

blood oxygenation data (e.g., BOLD fMRI) to include the relationship between the changes in blood oxygenation to the changes in the tissue mitochondria oxidative rate using a first-order model as performed in this work, bridging the gap between the tissue mitochondrial CMR_{O2} and the CMR_{O2}-driven changes in blood oxygenation.

Acknowledgements

The authors thank Michelle Tasker and Ping Wang for their technical assistance and Drs Ken Reinert and Timothy Ebner for providing valuable insight on flavoprotein autofluorescence imaging.

Disclosure/conflict of interest

The authors declare no conflict of interest.

References

Ances BM, Wilson DF, Greenberg JH, Detre JA (2001) Dynamic changes in cerebral blood flow, O2 tension, and calculated cerebral metabolic rate of O2 during functional activation using oxygen phosphorescence quenching. *J Cereb Blood Flow Metab* 21:511–6

Buxton RB, Uludag K, Dubowitz DJ, Liu TT (2004) Modeling the hemodynamic response to brain activation. *Neuroimage* 23 Suppl 1: S220–33

Chance B (1968) Cytochromes: chemical and structural aspects. *Science* 159:654–8

Chiarelli PA, Bulte DP, Piechnik S, Jezzard P (2007) Sources of systematic bias in hypercapnia-calibrated functional MRI estimation of oxygen metabolism. *Neuroimage* 34:35–43

Coq JO, Xerri C (1999) Tactile impoverishment and sensorimotor restriction deteriorate the forepaw cutaneous map in the primary somatosensory cortex of adult rats. *Exp Brain Res* 129:518–31

Davis TL, Kwong KK, Weisskoff RM, Rosen BR (1998) Calibrated functional MRI: mapping the dynamics of oxidative metabolism. *Proc Natl Acad Sci USA* 95:1834–9

Fatt I (1976) *The Polarographic Oxygen Sensor: Its Theory of Operation and Its Application in Biology, Medicine, and Technology*. Cleveland, OH: CRC Press

Fox PT, Raichle ME, Mintun MA, Dence C (1988) Nonoxidative glucose consumption during focal physiologic neural activity. *Science* 241:462–4

Fukuda M, Wang P, Moon CH, Tanifuji M, Kim SG (2006) Spatial specificity of the enhanced dip inherently induced by prolonged oxygen consumption in cat visual cortex: implication for columnar resolution functional MRI. *Neuroimage* 30:70–87

Hassinen I, Chance B (1968) Oxidation-reduction properties of the mitochondrial flavoprotein chain. *Biochem Biophys Res Commun* 31:895–900

Herman P, Sanganahalli BG, Blumenfeld H, Hyder F (2009) Cerebral oxygen demand for short-lived and steady-state events. *J Neurochem* 109(Suppl 1):73–9

Hertz L (2004) The astrocyte-neuron lactate shuttle: a challenge of a challenge. *J Cereb Blood Flow Metab* 24:1241–8

Horecker BL (1943) The absorption spectra of hemoglobin and its derivatives in the visible and near infra-red regions. *J Biol Chem* 148:173–83

Huang S, Heikal AA, Webb WW (2002) Two-photon fluorescence spectroscopy and microscopy of NAD(P)H and flavoprotein. *Biophys J* 82:2811–25

Huppert TJ, Allen MS, Diamond SG, Boas DA (2009) Estimating cerebral oxygen metabolism from fMRI with a dynamic multicompartment Windkessel model. *Hum Brain Mapp* 30:1548–67

Husson TR, Mallik AK, Zhang JX, Issa NP (2007) Functional imaging of primary visual cortex using flavoprotein autofluorescence. *J Neurosci* 27:8665–75

Kasischke KA, Vishwasrao HD, Fisher PJ, Zipfel WR, Webb WW (2004) Neural activity triggers neuronal oxidative metabolism followed by astrocytic glycolysis. *Science* 305:99–103

Kim SG, Rostrup E, Larsson HB, Ogawa S, Paulson OB (1999) Determination of relative CMRO2 from CBF and BOLD changes: significant increase of oxygen consumption rate during visual stimulation. *Magn Reson Med* 41:1152–61

L'Heureux B, Gurden H, Pain F (2009) Autofluorescence imaging of NADH and flavoproteins in the rat brain: insights from Monte Carlo simulations. *Opt Express* 17:9477–90

Masamoto K, Kim T, Fukuda M, Wang P, Kim SG (2007) Relationship between neural, vascular, and BOLD signals in isoflurane-anesthetized rat somatosensory cortex. *Cereb Cortex* 17:942–50

Masamoto K, Vazquez A, Wang P, Kim SG (2008) Trial-by-trial relationship between neural activity, oxygen consumption, and blood flow responses. *Neuroimage* 40:442–50

Nagaoka T, Zhao F, Wang P, Harel N, Kennan RP, Ogawa S, Kim SG (2006) Increases in oxygen consumption without cerebral blood volume change during visual stimulation under hypotension condition. *J Cereb Blood Flow Metab* 26:1043–51

Obata T, Liu TT, Miller KL, Luh WM, Wong EC, Frank LR, Buxton RB (2004) Discrepancies between BOLD and flow dynamics in primary and supplementary motor areas: application of the balloon model to the interpretation of BOLD transients. *Neuroimage* 21: 144–153

Offenhauser N, Thomsen K, Caesar K, Lauritzen M (2005) Activity-induced tissue oxygenation changes in rat cerebellar cortex: interplay of postsynaptic activation and blood flow. *J Physiol* 565:279–94

Pawlik G, Rackl A, Bing RJ (1981) Quantitative capillary topography and blood flow in the cerebral cortex of cats: an *in vivo* microscopic study. *Brain Res* 208:35–58

Pellerin L, Bouzier-Sore AK, Aubert A, Serres S, Merle M, Costalat R, Magistretti PJ (2007) Activity-dependent regulation of energy metabolism by astrocytes: an update. *Glia* 55:1251–62

Reinert KC, Dunbar RL, Gao W, Chen G, Ebner TJ (2004) Flavoprotein autofluorescence imaging of neuronal activation in the cerebellar cortex *in vivo*. *J Neurophysiol* 92:199–211

Riddle DR, Purves D (1995) Individual variation and lateral asymmetry of the rat primary somatosensory cortex. *J Neurosci* 15:4184–95

Shibuki K, Hishida R, Murakami H, Kudoh M, Kawaguchi T, Watanabe M, Watanabe S, Kouuchi T, Tanaka R (2003) Dynamic imaging of somatosensory cortical activity in the rat visualized by flavoprotein autofluorescence. *J Physiol* 549:919–27

Shulman RG, Hyder F, Rothman DL (2001) Lactate efflux and the neuroenergetic basis of brain function. *NMR Biomed* 14:389–96

Sirotin YB, Das A (2010) Spatial relationship between flavoprotein fluorescence and the hemodynamic response in the primary visual cortex of alert Macaque monkeys. *Front Neuroenergetics* 2:6

Smith AJ, Blumenfeld H, Behar KL, Rothman DL, Shulman RG, Hyder F (2002) Cerebral energetics and spiking frequency: the neurophysiological basis of fMRI. *Proc Natl Acad Sci USA* 99:10765–70

Thompson JK, Peterson MR, Freeman RD (2003) Single-neuron activity and tissue oxygenation in the cerebral cortex. *Science* 299:1070–2

Tohmi M, Kitaura H, Komagata S, Kudoh M, Shibuki K (2006) Enduring critical period plasticity visualized by transcranial flavoprotein imaging in mouse primary visual cortex. *J Neurosci* 26:11775–85

Vazquez AL, Masamoto K, Fukuda M, Kim SG (2010) Cerebral oxygen delivery and consumption during evoked neural activity. *Front Neuroenergetics* 2:11

Vazquez AL, Masamoto K, Kim SG (2008) Dynamics of oxygen delivery and consumption during evoked neural stimulation using a compartment model and CBF and tissue P(O2) measurements. *Neuroimage* 42:49–59

Weber B, Burger C, Wyss MT, von Schulthess GK, Scheffold F, Buck A (2004) Optical imaging of the spatiotemporal dynamics of cerebral blood flow and oxidative metabolism in the rat barrel cortex. *Eur J Neurosci* 20:2664–70

Zappe AC, Uludag K, Logothetis NK (2008) Direct measurement of oxygen extraction with fMRI using 6% CO2 inhalation. *Magn Reson Imaging* 26:961–7

Zheng Y, Martindale J, Johnston D, Jones M, Berwick J, Mayhew J (2002) A model of the hemodynamic response and oxygen delivery to brain. *Neuroimage* 16:617–37

Supplementary Information accompanies the paper on the Journal of Cerebral Blood Flow & Metabolism website (http://www.nature.com/jcbfm)